INFLUENCE OF ROLLING PROCESSES ON THE MICROSTRUCTURES AND MECHANICAL PROPERTIES OF A 19CR1.5MO0.5W FERRITIC STAINLESS STEEL*

Liqing Chen[1]
Houlong Liu[2]
Lingling Liu[3]
Mingyu Ma[4]
Weiping Tong[5]

Abstract
In this article, a 444-type heat-resistant ferritic stainless steel containing 0.05wt% Ce and 2wt% (Mo+W) was used as an experimental material and a study was carried out on the effect of rolling processes on the microstructures and texture evolution as well as on the mechanical properties and formability. The rolling processes contain hot rolling at different hot rolling finish temperatures, annealing after hot rolling, cold rolling and subsequent annealing. As for the hot rolling process, two hot rolling finish temperatures, 860 °C and 770 °C, were adopted, and their influence on the microstructures and mechanical properties was comparatively studied. The results showed that the microstructures after hot rolling and subsequent annealing could be refined by lowering the hot rolling finish temperature. The resultant microstructures after cold rolling and annealing were hereditarily refined. Lowering the hot rolling finish temperature can weaken the α-fiber texture in hot rolled or cold rolled ferritic stainless steel strip. However, the γ-fiber texture was homogeneously strengthened by annealing the cold rolled ferritic stainless steel strip. Enhanced mechanical property and formability in terms of strength and average plastic strain ratio could be obtained by lowering the hot rolling finish temperature of ferritic stainless steel.
Keywords: Ferritic stainless steel; Rolling processes; Microstructure; Texture; Mechanical properties; Formability.

[1] *PhD, Professor, State Key Laboratory of Rolling and Automation, Northeastern University, 3-11 Wenhua Road, Shenyang 110819, China.*
[2] *PhD Candidate, State Key Laboratory of Rolling and Automation, Northeastern University, 3-11 Wenhua Road, Shenyang 110819, China.*
[3] *Graduate student for Master's degree, State Key Laboratory of Rolling and Automation, Northeastern University, 3-11 Wenhua Road, Shenyang 110819, China.*
[4] *PhD Candidate, State Key Laboratory of Rolling and Automation, Northeastern University, 3-11 Wenhua Road, Shenyang 110819, China.*
[5] *PhD, Professor, Key Laboratory of Electromagnetic Processing of Materials (Ministry of Education), Northeastern University, 3-11 Wenhua Road, Shenyang 110819, China.*

** Technical contribution to the 11th International Rolling Conference, part of the ABM Week 2019, October 1st-3rd, 2019, São Paulo, SP, Brazil.*

1 INTRODUCTION

The cost-effective ultra-pure ferritic stainless steels have excellent anti-corrosion ability, thermal fatigue resistance and oxidation resistance at elevated temperatures [1, 2]. These advantages make ferritic stainless steels promising for manufacturing automotive exhaust manifold. The service temperature of traditional 444-type ferritic stainless steels used for exhaust manifold is ~900 °C. However, the need for the vehicle emission standard leads to an increased temperature for the exhaust manifold and its maximum service temperature will reach 950–1050 °C, or even up to 1100 °C [3]. In this case, the materials used for the next generation of automotive exhaust systems should possess excellent anti-oxidation ability and thermal fatigue resistance at elevated temperatures. It was reported that the addition of W and/or Mo could improve both the creep rupture strength and thermal fatigue resistance of ferritic stainless steel through precipitation and/or solid-solution strengthening effects [4–6]. In addition, it was confirmed that the oxide film became uniform and compact and the amount of defects at the oxide/metal interface were significantly reduced such that it displayed good scale adhesion after the addition of Ce [7, 8]. In order to improve the performance of the high temperature oxidation resistance and thermal mechanical fatigue behavior of manifold materials, alloying with rare earth element Ce and higher melting-point metals W and/or Mo may be an effective way.

Generally, the formability of the ferritic stainless steel should be taken into consideration in the practical application and this can be improved by several approaches, such as the chemical composition design [9], solidified microstructure control [10], and optimization of rolling schedules [11, 12]. Regarding the new developed heat-resistant ferritic stainless steel containing W+Mo and Ce, however, the influence of hot rolling processes on the formability and mechanical properties remains unclear and need to have a deep understanding. The aim of this study is to explore the effect of rolling processes on the microstructures and texture evolution of a 19Cr1.5Mo0.5W ferritic stainless steel as well as on its mechanical properties and formability. The enhanced formability and mechanical properties were also discussed on the basis of microstructural and texture evolution in association with the rolling processes.

2 EXPERIMENTAL

The chemical composition of the experimental steel is listed in Table 1. The steel ingots were prepared in a vacuum induction furnace and hot forged into slab with a thickness of 50 mm after heated at 1180 °C and held for 2 h. After reheated to 1200 °C and soaked for 1h, the slabs were hot rolled to plates of 5 mm in thickness wherein the finish temperatures were controlled at 860 °C and 770 °C. Then they were air-cooled and followed by annealing at 1050 °C for 5 min. Finally, these plates were cold rolled to the sheets of 1 mm in thickness and subsequently annealed at 1050 °C for 1 min.

Room temperature tensile tests were carried out by INSTRON 4206 tensile testing machine according to GB/T 228.1-2010 [13]. A tensile speed of 3 mm/min was employed for room temperature tensile tests to determine the mechanical properties including the tensile strength (σ_b), yield strength (σ_s), and elongation (ε). The formability characterized by plastic strain ratio (r), i.e. the ratio of the true strain in the width direction to the thickness direction, was measured according to GB/T5027-2016 [14]. A mean value of plastic strain ratios, r_m, was calculated by Equation 1 [15]:

$$r_m = 1/4(r_{0^\circ} + 2r_{45^\circ} + r_{90^\circ}) \quad (1)$$

The anisotropy of plastic strain ratio is called Δr and calculated according to Equation 2:

$$\Delta r = 1/2(r_{0^\circ} - 2r_{45^\circ} + r_{90^\circ}) \quad (2)$$

where the subscripts 0°, 45° and 90° refer to the directions at which the sample was taken relative to the rolling direction. The formability of the ferritic stainless sheet could be evaluated based on these data. In addition, the surface roughness R_a and maximum surface roughness R_t of the final sheets strained by 15% along the rolling direction was measured by a TR 300 roughness measuring instrument.

The specimens for the texture measurement were mechanically polished and etched in a solution of dilute hydrochloric acid (HCl) to remove the deformed layer. In this study, all the textures were measured at the central layer of the sheets to characterize the textural evolution in Bruker D8 Discover X-ray diffractometer with CoKα radiation. The texture analysis was performed via the measurement of 3 incomplete pole figures {110}, {200}, and {211} on the central layer of the sheet, and the orientation distribution function (ODF) was calculated for these three pole figures using the series expansion method with L_{max}=22. The ODF was presented as plots of φ2=45° sections in Euler space defined by the Euler angles (φ_1, Φ, φ_2). Figure 1 shows the positions of typical orientations in $\varphi_2 = 45°$ ODF section that contains the texture components discussed in this study. The orientation density $f(g)$ is plotted against the Euler angles φ_1 and Φ.

The metallographic specimens were etched in a solution of 5 g $FeCl_3$+50 ml HCl+150 ml H_2O and then an optical microscope (BX53M) was used for microstructural observation and analysis. The crystal orientation distribution and average grain size of the samples were measured using FEI Quanta 600 scanning electron microscope (SEM) equipped with EBSD detector. In this study, EBSD was applied on the longitudinal sections as defined by the rolling direction (RD) and the normal direction (ND).

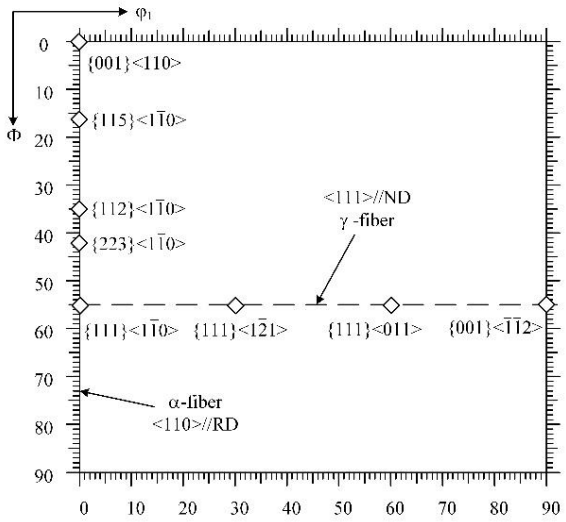

Figure 1. Typical orientations of the ferritic stainless steels in $\varphi_2 = 45°$ ODF section.

Table 1. Chemical composition of the experiment steel (wt %)

C	Si	Mn	Cr	Nb	Ti	N	Mo	W	Ce	Fe
<0.01	0.44	0.34	19.6	0.47	0.14	<0.009	1.55	0.45	0.05	Bal.

3 RESULTS AND DISCUSSION

3.1 Microstructure and texture evolution

The optical micrographs for the microstructures in the hot rolled and annealed sheets are shown in Figure 2. The microstructures in the two steels were both elongated along the rolling direction after hot rolling. However, the banded structures in the hot rolled plate with a hot rolling finish temperature of 770 °C (Figure 2(b)) were narrower than that in the hot rolled plate with a hot rolling finish temperature of 860 °C (Figure 2(a)), which indicated that work hardening was severer

for the hot rolled plate with lower hot rolling finish temperature. After annealed at 1050 °C for 5 min, the microstructures in annealed sheets were consisted of a single ferritic phase and the recrystallized grains in the hot rolled sheet with a hot rolling finish temperature of 770 °C was finer than that in the other one.

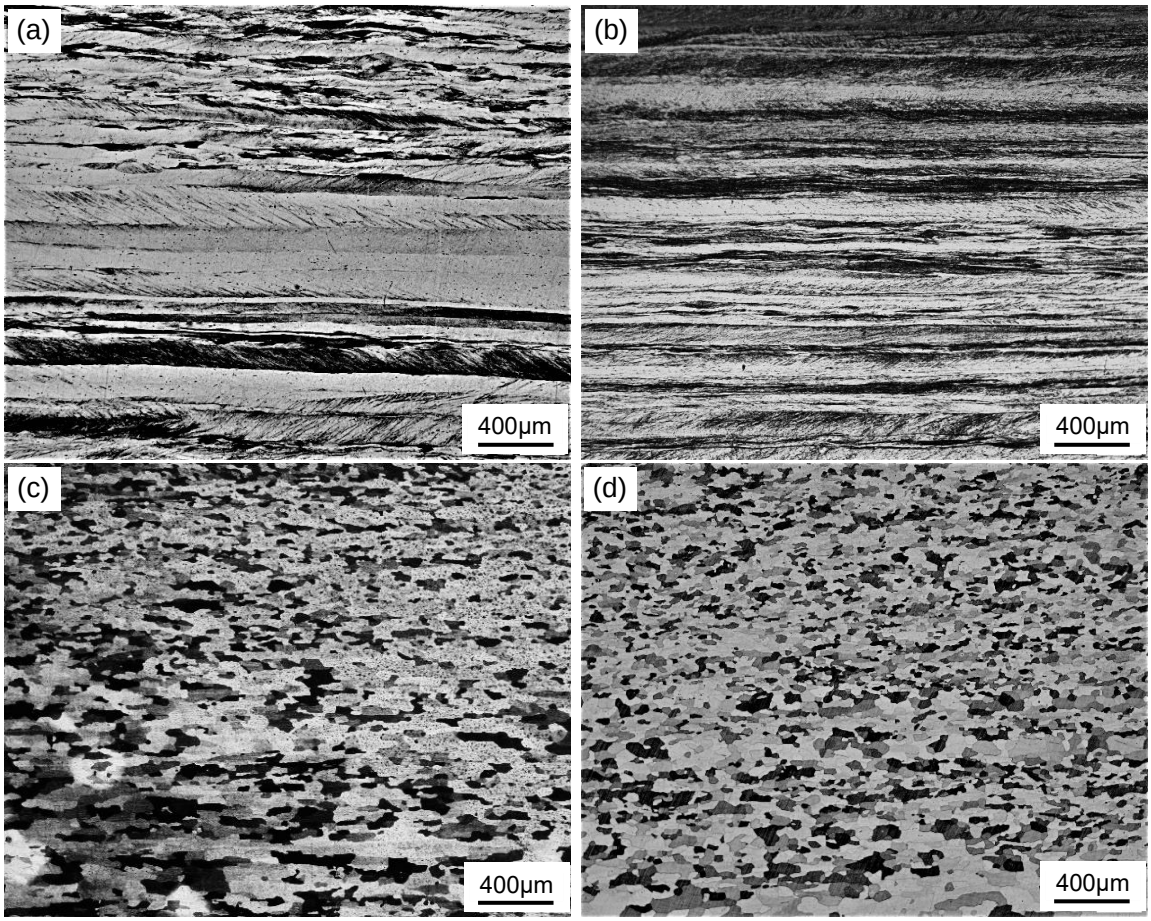

Figure 2. Optical micropraphs showing the microstructure for the hot rolled sheet (a) and annealed sheet (c) with hot rolling finish temperature of 860 °C and for the hot rolled sheet (b) and annealed sheet (d) with hot rolling finish temperature of 770 °C.

Figure 3 shows the microstructures in cold rolled sheets and corresponding annealed sheets. The microstructures in two cold rolled sheets were elongated. Nevertheless, there were narrower and more banded structures in the cold rolled plate with lower hot rolling finish temperature, leading to the fine recrystallization grains in subsequent annealed sheet. The average grain sizes of the annealed sheets with the hot rolling finish temperature of 860 °C and 770 °C were 33. 4 μm and 20.8 μm, respectively.

When the hot rolling finish temperature was decreased, the dynamic recovery was inhibited and work hardening and deformation stored energy were increased, which provided the large number of nucleation sites and the driving force for recrystallization. The microstructures in the hot rolled plate were thus refined after annealing. After cold rolling, it could be inherited to the microstructures of the cold rolled sheet causing refined grains in the final plate.

Figure 4 displays the textures of the central layers in the hot rolled and annealed sheets with different hot rolling finish temperatures. Obviously, the textures at the central layer of the hot rolled steels were mainly composed of the typical α-fiber. The intensity of α-fiber texture in the hot rolled sheet with a hot rolling finish temperature of 860 °C (Figure 4(a)) was

more intense compared with that of hot rolled sheet with a hot rolling finish temperature of 770 °C (Figure 4(b)). After annealing of the hot rolled sheet with hot rolling finish temperature of 860 °C (Figure 4(c)), the α-fiber texture of {115} <1$\bar{1}$0> shifted to {223}<1 $\bar{1}$ 0> and the corresponding intensity declined compared with that of {115} <1 $\bar{1}$ 0>, and the component of γ-fiber at {111}<1 $\bar{2}$ 1> distinctly appeared in the central layer of the hot rolled sheet after annealing. However, the annealed sample with a hot rolling finish temperature of 770 °C (Figure 4(d)) demonstrated that the intensity of the overall textures was weak. The reason may be that the deformation stored energy of the ferritic grain in hot rolled sheet was increased though lowering the hot rolling finish temperature, which made recrystallization easier for the grains of various orientations.

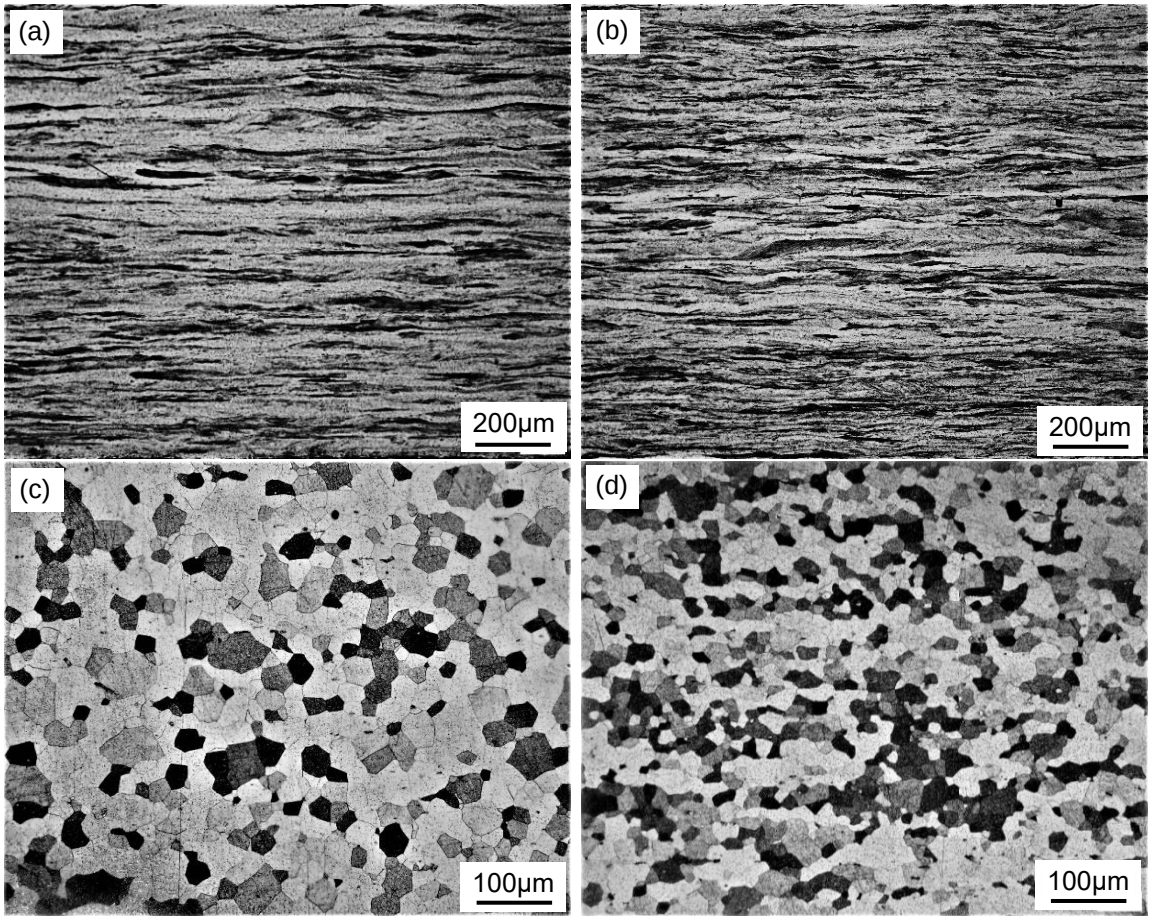

Figure 3. Optical micrographs showing the microstructures for the cold rolled sheet (a) and annealed sheet (c) with a hot rolling finish temperature of 860 °C and for the cold rolled sheet (b) and annealed sheet (d) with a hot rolling finish temperature of 770 °C.

Figure 5 shows the textures at the central layers of the cold rolled and annealed sheets with different hot rolling processes. The texture of cold rolled sheet mainly contained α-fiber and γ-fiber. The maximum intensities of the α-fiber in two cold rolled sheets were both located at {223} <1$\bar{1}$0>, but the intensity of α-fiber in cold rolled sheet with a hot rolling finish temperature of 860 °C was more stronger than that in the cold rolled sheet with a hot rolling finish temperature of 770 °C. Furthermore, the maximum intensities of the γ-fiber in cold rolled sheet with a hot rolling finish temperature of 860 °C were located at {111}< $\bar{1}\bar{2}$ 3>. However, the maximum intensities of the γ-fiber in cold rolled sheet with a hot rolling finish

temperature of 770 °C were located at {111}<0 $\bar{1}$ 1> and slightly increased when compared with that of the cold rolled sheet with a hot rolling finish temperature of 860 °C. After annealing, the recrystallization texture of the annealed sheet with a hot rolling finish temperature of 860 °C was mainly composed of the near γ-fiber at {111}<1 $\bar{2}$ 1> and {111}< $\bar{1}\bar{1}$ 2>, and the maximum intensity was about $f(g)_{max}$=7.5. The other one displayed a similar distribution of γ-fiber texture and the maximum intensity of {111}< $\bar{1}\bar{1}$ 2> was about $f(g)_{max}$ =10.1.

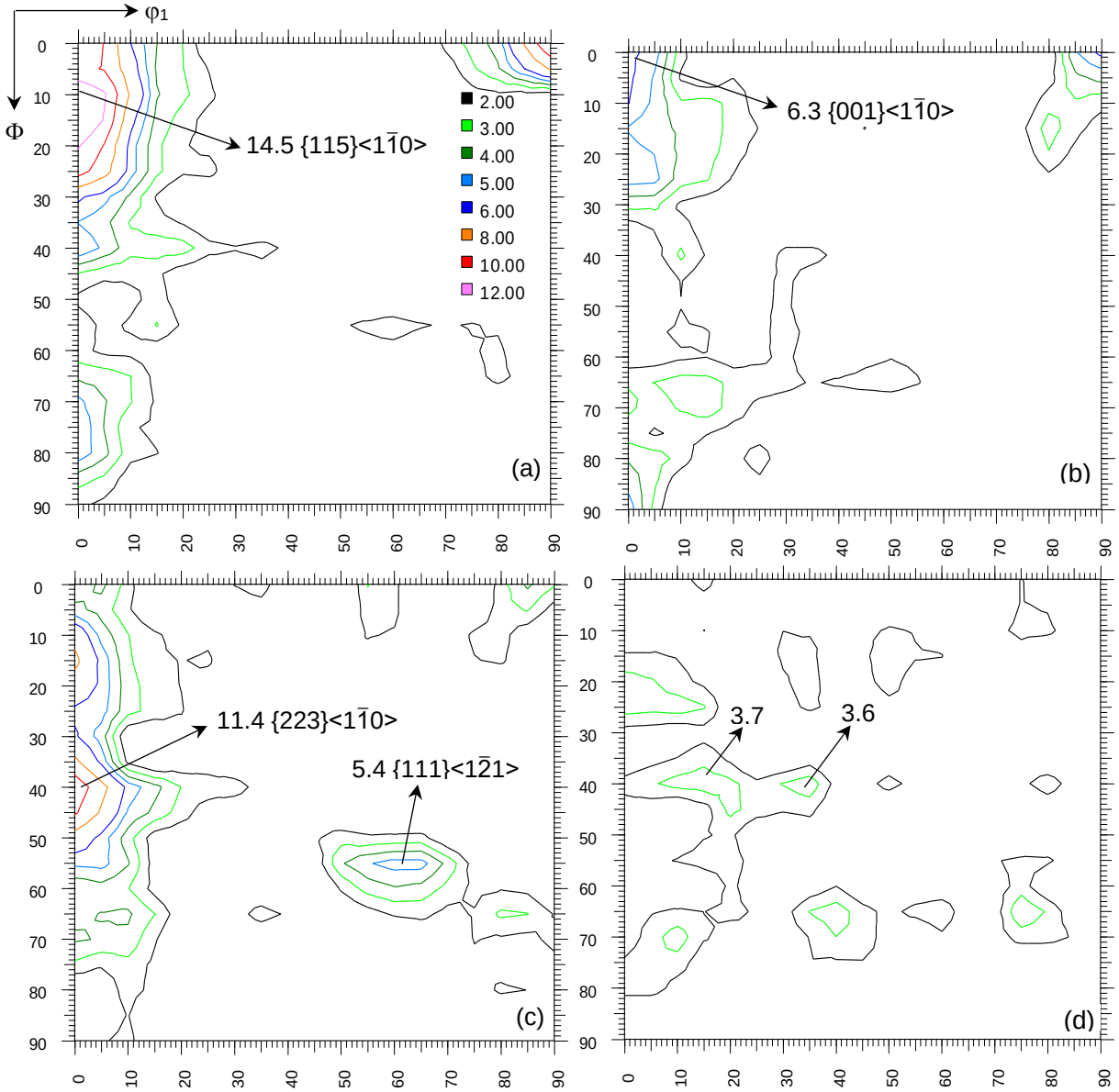

Figure 4. Constant φ_2=45° ODF sections for the hot rolled sheet (a) and annealed sheet (c) at hot rolling finish temperature of 860 °C and for the hot rolled sheet (b) and annealed sheet (d) at hot rolling finish temperature of 770 °C.

The textures in hot rolled and annealed sheet can be inherited to cold rolled sheet to a certain extent [16]. The stronger the intensity of the hot-rolled and annealed sheet was, the stronger the intensity of α-fiber texture in the cold rolled sheet was. During annealing of the cold rolled sheet, the recrystallization grains with γ-fiber orientation grew up gradually and annexed the grain with α-fiber orientation [17].

Therefore, lowering hot rolling finish temperature can lead to a reduction in intensity of the α-fiber texture and an increase of the γ-fiber texture intensity in the cold rolled sheet, which was beneficial to the formation of γ-fiber texture in the cold rolled sheet after annealing.

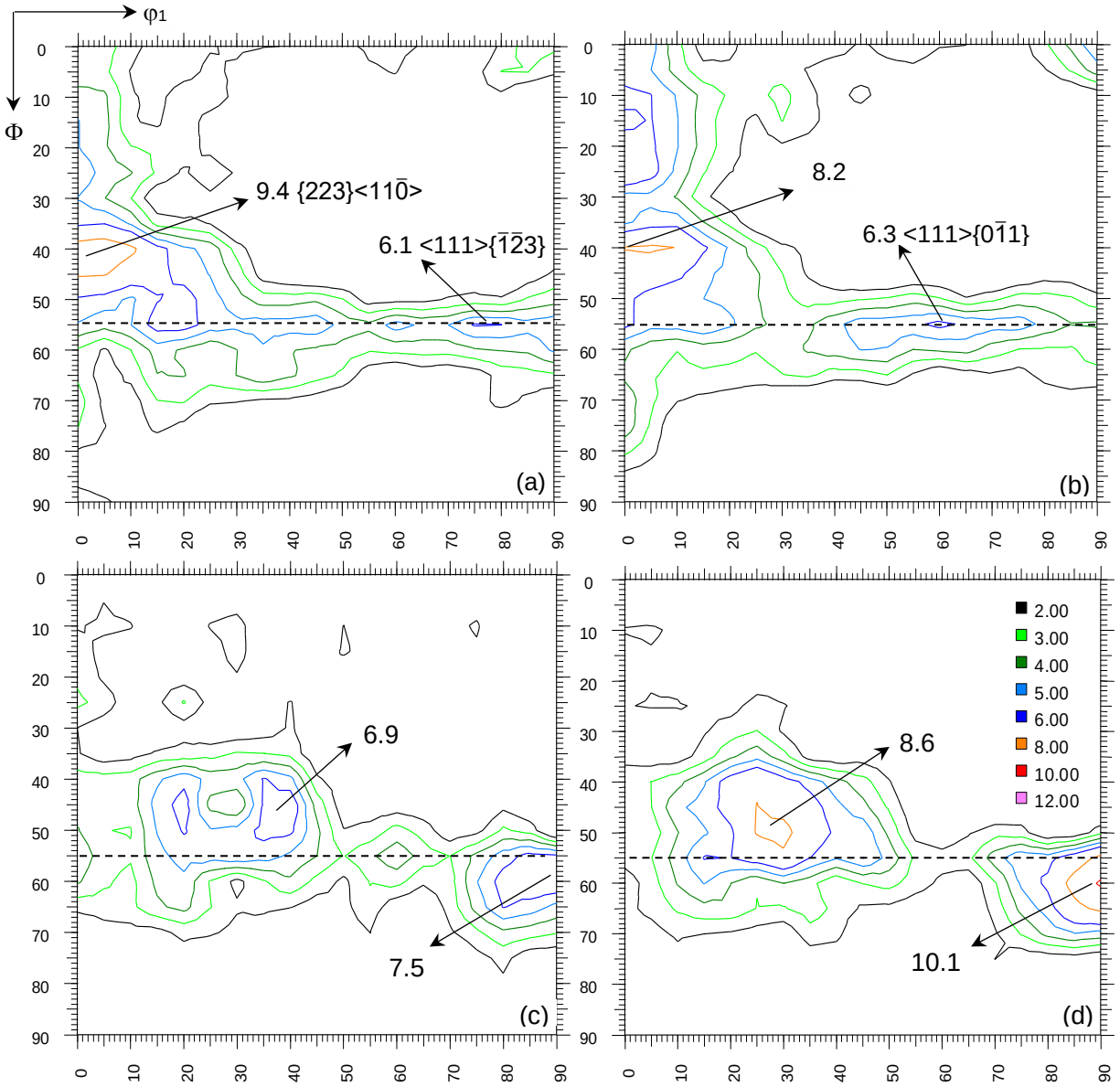

Figure 5. Constant φ_2=45° ODF sections for the cold rolled sheet (a) and annealed sheet (c) with a hot rolling finish temperature of 860 °C and for the cold rolled sheet (b) and annealed sheet (d) with a hot rolling finish temperature of 770 °C.

The grain orientation distribution of the longitudinal section in cold rolled sheet after annealing at 1050 °C for 1 min examined by EBSD is shown in Figure 6. The proportion of blue and near blue crystals ({111}//ND) in annealed sheet with a hot rolling finish temperature of 860 °C was larger than that of other color crystals. However, the distribution of blue and near blue grains in the direction of thickness was obviously uneven, and those in the middle area were relatively more than nearby the surface layer. Yet, it can be clearly observed that the different orientation grains in annealed sheet with a hot rolling finish temperature of 770 °C

were distributed uniformly in the direction of the thickness. It can be concluded that decreasing the hot rolling finish temperature can make the distribution of various orientation grains more homogeneous in cold rolled sheet after annealing.

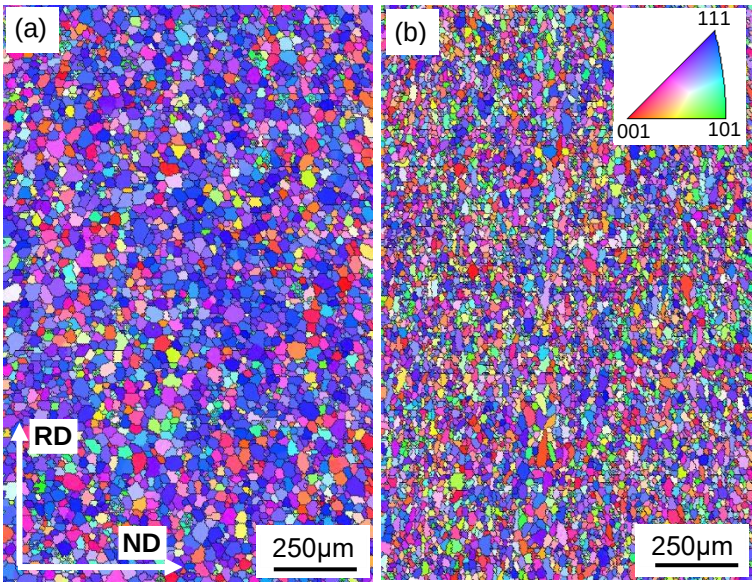

Figure 6. Crystal orientation maps of the annealed sheet with the hot rolling finish temperatures of 860 °C (a) and 770 °C (b).

Table 2. Mechanical properties of the cold rolled and annealed sheets under two hot rolling conditions

hot rolling finish temperature/°C	yield strength σ_s/MPa	tensile strength σ_b/MPa	elongation δ/%	yield strength ratio
860	354	527	32.1	0.67
770	367	542	32	0.68

Table 3. Formability of cold rolled and annealed sheets with two hot rolling processes

hot rolling finish temperature/°C	r_0	r_{45}	r_{90}	r_m	Δr	R_a/μm	R_t/μm	n
860	1.64	0.95	1.36	1.36	0.82	0.538	4.138	0.21
770	1.84	1.36	1.51	1.52	0.32	0.352	2.673	0.21

3.2 Mechanical properties and formability

Table 2 shows the mechanical properties for the cold rolled and annealed sheets with different hot rolling finish temperatures. With decreasing the hot rolling finish temperature, both of the yield strength and tensile strength of annealed sheets were increased. However, the changes of the yield strength ratio and elongation were not obvious. An increase of the strength can be attributed to the grain refinement by lowering the hot rolling finish temperature.

Table 3 presents the formability data of cold rolled and annealed sample under different hot rolling conditions. Work hardening index n of two final sheets was equal in value. The r value of annealed sheet in different directions was increased with the decrease of the hot rolling finish temperature, especially significantly

increased by 43.2% in 45° direction. Not only the r_m value was enhanced, but the Δr value was reduced by 61.6% as well. Deep drawability can be evaluated by r_m and Δr values and the condition leading to a better deep drawing operation is that there is a higher r_m value and Δr value is close to zero [18, 19]. Hence, the cold rolled and annealed sheet with a hot rolling finish temperature of 770 °C possess a better deep drawability. The average surface roughness R_a and maximum surface roughness R_t of cold rolled and annealed sheets after 15% tensile deformation are also presented in Table 3. Both of the average surface roughness R_a and maximum surface roughness R_t of cold rolled and annealed sheet were obviously reduced by lowering the hot rolling finish temperature, so the surface quality of the finished sheet was improved.

It was confirmed that higher plastic strain ratio and lower anisotropy were displayed by materials having a very intense γ-fiber texture at {111}<1$\bar{2}$1> and {111}<$\bar{1}\bar{1}$2> in the steel sheet [20, 21] and this phenomenon was advantageous for drawing operations and the forming limits [22, 23]. In addition, the surface defect problem of ridging was unfavorable for surface appearance and further drawing operations. Shin et al. [24] suggested that the ridging of the ferritic stainless steel was mainly resulted from different plastic deformation of the grains with different crystal orientations when subjected to tension, and the longitudinal alignment of grain clusters could also lead to the formation of a corrugated surface [25]. Moreover, Ma et al. [26] also revealed that the grain refinement was effective in reducing the ridging height of ferritic stainless steel during the forming process. From this work, we can understand that the formability of the ferritic stainless steel can be significantly improved as long as high intensity γ-fiber texture, refinement of microstructure and dispersed distribution of recrystallized grains with various orientations were developed after cold rolling and annealing.

4 CONCLUSIONS

(1) For 19Cr1.5Mo0.5W heat-resistant ferritic stainless steel, lowering the hot rolling finish temperature can refine the microstructure in final annealed sheet and increase the yield and tensile strengths. It can also make the grain distribution of various orientions homogeneous along the direction of thickness.

(2) The intensity of α-fibers texture in hot rolled sheet can be effectively decreased by lowering the hot rolling finishing temperature. This characteristic can be inherited to cold rolled sheet, resulting in an increase of the intensity of γ-fibers texture after annealing.

(3) The cold rolled and annealed stainless steel with hot rolling finish temperature of 770 °C exhibited excellent formability due to the occurrence of strong γ-fiber texture and dispersed distribution of recrystallized grains with various orientations.

Acknowledgments

The authors gratefully acknowledge the joint financial support from the National Natural Science Foundation of China and Baowu Steel Group Co., Ltd. (Grant No. U1660205).

REFERENCES

1 Ma MY, He CL, Chen LQ, Wei LL, Misra RDK. Effect of W and Ce additions on the electrochemical corrosion behavior of 444-type ferritic stainless steel. Corros. Eng. Sci. Technol. 2018, 53(3): 199-205.

2 Safikhani A, Aminfard M. Effect of W and Ti addition on oxidation behavior and area-specific resistance of Fe-22Cr-0.5Mn ferritic stainless steel for SOFCs interconnect. Int. J. Hydrogen Energy, 2014, 39(5): 2286-2296.

3 Faivre L, Santacreu PO, Acher A. A new ferritic stainless steel with improved thermo-mechanical fatigue resistance for

exhaust parts. Mater. High. Temp. 2013, 30(1): 36-42.
4 Fujita N, Ohmura K, Yamamoto A. Changes of microstructures and high temperature properties during high temperature service of Niobium added ferritic stainless steels. Mater. Sci. Eng. A 2003, 351: 272-281.
5 Chiu YT, Lin CK. Effects of Nb and W additions on high-temperature creep properties of ferritic stainless steels for solid oxide fuel cell interconnect. J. Power Sources 2012, 198: 149-157.
6 Froitzheim J, Meier GH, Niewolak L, Ennis PJ, Hattendorf H, Singheiser L, Quadakkers WJ. Development of high strength ferritic steel for interconnect application in SOFCs. J. Power Sources 2008, 178: 163-173.
7 Wei LL, Zheng JH, Chen LQ, Misra RDK. High temperature oxidation behavior of ferritic stainless steel containing W and Ce. Corros. Sci. 2018, 142: 79-92.
8 Wei LL, Chen LQ, MA MY, Liu HL, Misra RDK. Oxidation behavior of ferritic stainless steels in simulated automotive exhaust gas containing 5vol.% water vapor. Mater. Chem. Phys. 2018, 205: 508-517.
9 Du W, Jiang L, Sun Q, Liu Z, Zhang X. Effect of hot band annealing processes on microstructure, texture and *r*-value of ferritic stainless steel. J. Iron Steel Res. Int. 2010, 17(7): 58-62.
10 Zhang X, Fan LJ, Xu YL, Li J, Xiao XS, Jiang LZ. Effect of aluminum on microstructure, mechanical properties and pitting corrosion resistance of ultra-pure 429 ferritic stainless steels. Mater. Des. 2015, 65: 682-689.
11 Huh MY, Engler O. Effect of intermediate annealing on texture, formability and ridging of 17%Cr ferritic stainless steel sheet. Mater. Sci. Eng. A 2001, 308(1): 74-87.
12 Abreu HFG, Bruno ADS, Tavares SSM, Santos RP, Carvalho SS. Effect of high temperature annealing on texture and microstructure on an AISI-444 ferritic stainless steel. Mater. Charact. 2006, 57(4): 342-347.
13 GB/T 228.1-2010, Metallic materials-tensile testing-Part 1: Method of test at room temperature, China Standard Press, 2010.
14 GB/T 5027-2016, Metallic materials–sheet and strip–determination of plastic strain ratio, China Standard Press, 2016.
15 Zhang X, Fan LJ, Xu YL, Li J, Xiao XS, Jiang LZ. Texture, microstructure and mechanical properties of aluminum modified ultra-pure 429 ferritic stainless steels. Mater. Des. 2016, 89: 626-635.
16 Liu HL, Ma MY, Liu LL, Wei LL, Chen LQ. Effect of Hot Band Annealing Processes on Texture and Formability of 19Cr2Mo1W Ferritic Stainless Steel. Acta Metall. Sin. 2019, 55(5): 566-574.
17 Sinclair CW, Robaut F, Maniguet L, Mithieux JD, Schmitt JH, Brechet Y. Recrystallization and texture in a ferritic stainless steel: an EBSD study. Advanced Eng. Mater. 2003, 5(8): 570-574.
18 Bai Y, He T, Liu YD. Effects of Sn microalloying on cold rolling and recrystallization textures and microstructure of a ferritic stainless steel. Mater. Charact. 2018, 137: 142-150.
19 Cai GJ, Li CS, Wang DG, Zhou YK. Investigation of annealing temperature on microstructure and texture of Fe-19Cr-2Mo-Nb-Ti ferritic stainless steel. Mater. Charact. 2018, 141: 169-176.
20 Li JX, Liu ZY, Gao CR, Wang ZD, Liu XH, Wang GD. Evolution of textures in interstitial free steel during multiple cold rolling and annealing. J. Mater. Process. Technol. 2005, 167(1): 132-137.
21 Fu JW, Li F, Sun JJ, Wu YC. Texture, orientation, and mechanical properties of Ti-stabilized Fe-17Cr ferritic stainless steel. Mater. Sci. Eng. A 2018, 738: 335-343.
22 Xu L, Barlat F, Ahn DC, Bressan JD. Forming limit and fracture mechanism of ferritic stainless steel sheets. Mater. Sci. Eng. A 2011, 528(7): 3113-3121.
23 Du W, Jiang LZ, Sun QS, Liu ZY, Zhang X. Microstructure, Texture, and Formability of Nb+Ti Stabilized High Purity Ferritic Stainless Steel. J. Iron Steel Res. Int. 2010, 17(6): 47-52.
24 Shin HJ, An JK, Park SH, Lee DN. The effect of texture on ridging of ferritic stainless steel. Acta Mater. 2003, 51(16): 4693-4706.
25 Ma XG, Zhao JW, Du W, Zhang X, Jiang LZ, Jiang ZY. An analysis of ridging of ferritic stainless steel 430. Mater. Sci. Eng. A 2017, 685: 358-366.

26 Ma XG, Zhao JW, Du W, Zhang X, Jiang ZY. Effects of rolling processes on ridging generation of ferritic stainless steel. Mater. Charact. 2018, 137: 201-211.